Polymer 97 (2016) 11–19

Contents lists available at ScienceDirect

Polymer

journal homepage: www.elsevier.com/locate/polymer

Electrically conductive thermoplastic polyurethane/polypropylene nanocomposites with selectively distributed graphene

Yan Lan [a], Hu Liu [a, b], Xiaohan Cao [a], Shuaiguo Zhao [a], Kun Dai [a, **], Xingru Yan [b], Guoqiang Zheng [a], Chuntai Liu [a], Changyu Shen [a], Zhanhu Guo [b, *]

[a] School of Materials Science and Engineering, The Key Laboratory of Material Processing and Mold of Ministry of Education, Zhengzhou University, Zhengzhou, Henan 450001, PR China
[b] Integrated Composites Laboratory (ICL), Department of Chemical & Biomolecular Engineering, University of Tennessee, Knoxville, TN 37996, USA

ARTICLE INFO

Article history:
Received 19 March 2016
Received in revised form
28 April 2016
Accepted 6 May 2016
Available online 9 May 2016

Keywords:
Graphene
Nanocomposites
Co-continuous structure

ABSTRACT

The electrically conductive nanocomposites composing of different concentrations (0.05–1.5 wt%) of reduced graphene oxide (RGO) in the thermoplastic polyurethane/polypropylene (TPU/PP, 55/40) matrix with a fine co-continuous structure were fabricated by solution-flocculation and melt-mixing process using a micron twin-screw extruder. Both thermodynamic and kinetic theoretical analysis predicated the preferential location of RGO in the TPU rather than PP phase. Both optical microscope and field emission scanning electron microscopy (FESEM) observations verified this theoretical dispersion predication. The homogeneous dispersion of RGO in the TPU matrix is confirmed by wide-angle X-ray diffraction (WAXD) patterns and transmission electron microscope (TEM) observation. A very low percolation threshold of 0.054 wt% was achieved owing to high conductivity of RGO and favorable double percolation effect. The tensile strength and elongation at break of the composites with RGO content of only 0.5 wt% were improved by 341.9% and 354.3%, respectively. The present work provides a guideline for an efficient, facile fabrication technique of graphene based conductive polymer nanocomposites with high electrical conductivity and improved mechanical properties.

1. Introduction

Graphene, an atomically thick, two-dimension sheet composed of sp^2 carbon atoms arranged in honeycomb structure [1], has tremendous advantageous properties such as high electrical conductivity, extremely high specific surface area, favorable dispersibility in organic solvents, and high mechanical properties. Graphene has been utilized to tune the performances of polymer materials, like the mechanical strength, electrical property and thermal conductivity. Generally, high loading of conductive fillers, such as carbon black (CB) or graphite, *etc.*, is needed to make insulating polymers conductive, causing a high electrical percolation threshold. Up to now, much effort has been devoted to lower the percolation threshold. One important approach is to introduce highly conductive fillers with high aspect ratio (such as carbon nanotubes (CNTs), Ag nanowires, *etc.*), in other words, using lower filler contents to achieve higher electrical conductivity. Another way is to design the microstructure of conductive polymer composites (CPCs), for example, the double percolation structure, which was first introduced by Sumita et al. [2], and this concept has been applied to CB [3–6] and CNTs [7–12] filled CPCs. The term of double percolation means that both the percolation of conductive fillers in one given single polymer phase and the percolation of continuous conductive polymer composite phase in a polymer blend through the whole system take place simultaneously. The nanofillers are envisioned to be selectively located in one special phase or at the interface of the polymer blend system.

The selective dispersion behavior of nanofillers in the polymer blend is most commonly interpreted by thermodynamic and kinetic factors. A convenient and effective strategy to produce polymeric materials with double-percolation structure, *i.e.* the co-continuous structure, is the blending of two immiscible polymer components. For example, Pötschke et al. [13] reported the MWCNTs/polycarbonate (PC, 60 wt%)/poly(styrene-acrylonitrile) (SAN, 40 wt%) composites with a percolation threshold of 0.5 wt%, and the MWCNTs were thermodynamically driven to locate in the

* Corresponding author.
** Corresponding author.
E-mail addresses: kundai@zzu.edu.cn (K. Dai), zguo10@utk.edu (Z. Guo).

http://dx.doi.org/10.1016/j.polymer.2016.05.017
0032-3861/

PC domain. What's more, the formation of a co-continuous structure strongly depends on the melt viscosity ratio of the matrices. For example, Tassin et al. [14] studied the morphology evolution of CB/polypropylene (PP)/poly (ε-caprolactone) (PCL) composites induced by the change of viscosity ratio through using the polymers of different densities. For CB/PP/PCL (60w/40w) composites, a more elongated and interconnected structure of PCL was formed when the viscosity ratio was 0.3 and 1.1, and a circular structure was formed when the viscosity ratio was 0.06, 3.5 and 14.7.

As excellent conductive fillers with high specific surface area (SSA), graphene has also been applied to build a double percolation system [15–18]. However, the reported graphene based CPCs are always fabricated through solution mixing [16–18] or melt-compounding [15] techniques. For example, Zhu et al. [16] prepared the polystyrene/poly(methyl methanol)/octadecylamine-functionalized graphene (PS/PMMA/GE-ODA) composites by solution blending. The co-continuous structure was formed only when the component ratio was fixed at 50w/50w, and GE-ODA was selectively distributed in PS, then the composites exhibited an extremely low percolation threshold of 0.5 wt%. For the composites prepared by simple melt-mixing process, it is hard to achieve uniform dispersion in the matrix. Moreover, the agglomerations would act as defects in the composites and thus produced detrimental influence on the mechanical and electrical properties of the composites. Solution mixing technique undoubtedly involves low efficiency, small-scale production and narrow application range. However, there are still some advantages of solution mixing and melt-mixing, and these advantages are presented as follows. As for the solution mixing process, the nanofillers can be dispersed homogeneously in the polymer matrix under sonication treatment. Melt-mixing with twin-screw extruder possesses the advantages of low-cost, high-production, high-efficiency and easy manipulation. Importantly, the composite melt can also be directly molded into products using extrusion technique. Hence, melt-mixing with extruder provides a good foundation for the preparation and processing of conductive nanofillers based polymer composites. This feature cannot be easily realized by using simple solution method. Therefore, it is of great significance to develop a technique that combines the advantages of both melt-mixing and solution mixing for nanocomposites preparation. Up to now, the graphene based polymer nanocomposites prepared by solution-melt mixing method have not been reported yet, and it is even rare for the immiscible polymer composites.

In this work, immiscible thermoplastic polyurethane (TPU) and polypropylene (PP) are selected as polymer matrices because of their large differences in polarity and high interfacial tension. A series of co-continuous reduced graphene oxide (RGO)/TPU/PP composites were prepared by using a combined solution-flocculation and melt-mixing with a miniature twin-screw extruder, Wide-angle X-ray diffraction (WAXD) patterns and transmission electron microscope (TEM) measurements were applied to illustrate the dispersion levels of RGO in the polymer matrix. Wetting coefficient calculation was carried out to predict the selective location of RGO in the blend. The dispersion state of RGO, the microstructure of the CPC, and the RGO loading on the electrical and mechanical properties were investigated in details.

2. Experimental

2.1. Materials

Thermoplastic polyurethane (TPU, Elastollan 1185A) and polypropylene (PP, T30s) were used as polymer matrices. TPU with a density of 1.12 g/cm^3 and melt flow index of 17.5 g/10 min (215 °C, 10 Kg) was purchased from BASF Co. Ltd., Germany. PP with a density of 0.91 g/cm^3 and melt flow index of 3.0 g/10 min (210 °C, 2.16 Kg) was a commercial product of Maoming Petroleum Co., Guangdong, China. Reduced graphene oxide (RGO) solution with 0.5 wt% RGO (Chengdu Organic Chemicals Co. Ltd. Chengdu, China) was applied as electrical conductive filler. The graphene nanosheets of RGO solution have a SSA of 500–1000 m^2/g, thickness of 0.55–3.74 nm (Fig. 1a′) and size of about 0.5–3 μm. Maleic anhydride grafted polypropylene (MA-g-PP) (Nanjing Poly Star Polymer Materials Co. Ltd., China) was used as compatibilizer to enhance the compatibility between two matrices, its grafting percent was about 0.8–1.0%. Methanol and *N*,*N*-dimethyl formamide (DMF) were supplied by Zhiyuan Reagent Co. Ltd. Tianjin, China. All the chemicals were used as received without any further treatment.

TPU is a linear, segmented copolymer consisting of hard and soft segments. The hard segment usually consists of urethane groups, and the soft segment is typically a polyether-diol. PP is a kind of non-polar semi-crystallization polyolefin. For the chemical structure of MA-g-PP, it is composed of non-polar backbone and polar maleic anhydride branch chains. Specially, the addition of MA-g-PP has two counter-balancing effects, *i.e.*, lower the melt viscosity of PP and increase the polarity of PP phase. For one thing, the addition of MA-g-PP can lower the melt viscosity of PP to some extent, which make the melt viscosity of TPU and PP comparative. This can effectively improve the compatibility between TPU and PP phase. For another, the non-polar chain backbone of MA-g-PP intertwines with molecular chains of PP through van de Waals' force, and the maleic anhydride of MA-g-PP interacts with the TPU phase. The interaction between TPU and PP is enhanced under the help of MA-g-PP, which is in favor of the mutual diffusion of polymer chain segments. Finally, the interfacial adhesion between these two phases is enhanced.

2.2. Composite sample preparation

TPU was dried in a vacuum oven at 80 °C for 12 h prior to mixing. The composites fabrication process involved solution-flocculation and melt-mixing, schematically shown in Fig. 1(a) and (b), respectively. Briefly, 3.0 g of TPU was dissolved in 50 mL DMF by vigorous stirring for 1 h, meanwhile, the required amount of RGO solution was mixed with 45 mL DMF and treated under sonication for 30 min to create a homogeneous dispersion. Then TPU/DMF mixed with the RGO/DMF by stirring and sonication for another 30 min respectively. The energy input of sonication was fixed at 295 W. The flocculation and vacuum filtration processes were then carried out with the mixture to obtain a RGO/TPU premix, the volume ratio of the mixture and methanol was fixed at 1:5; the RGO/TPU was rinsed with methanol after filtration and then collected by drying in a vacuum oven at 80 °C for 24 h to remove the residual solvents. This process conquered the disadvantages of conventional one-step melt-mixing method for poor filler dispersion and inferior mechanical properties. Uniform dispersion of RGO in the TPU matrix through solution-flocculation process is of significant importance for the enhancement of electrical and mechanical properties of the composites. Subsequently, RGO/TPU, PP and MA-g-PP were melt-mixed by using a micron twin-screw extruder (L/D = 16) (SJSZ-10A, Wuhan Ruiming Plastic Machinery Co., Ltd) at a temperature of 200 °C and a rotation speed of 50 rpm. The extruded strands were collected and cut into small granules. The weight ratio of TPU/PP/MA-g-PP was fixed at 55/40/5 to produce a fine co-continuous structure in the polymer blend. Finally, the resulting granules were compressed into sheets with a thickness of ~0.5 mm by a vacuum mold pressing machine (FM450, Beijing Future Material Sci-tech Co., Ltd.) at 200 °C and 2.5 MPa for 5 min.

The used conductive nanofillers here were aqueous suspension

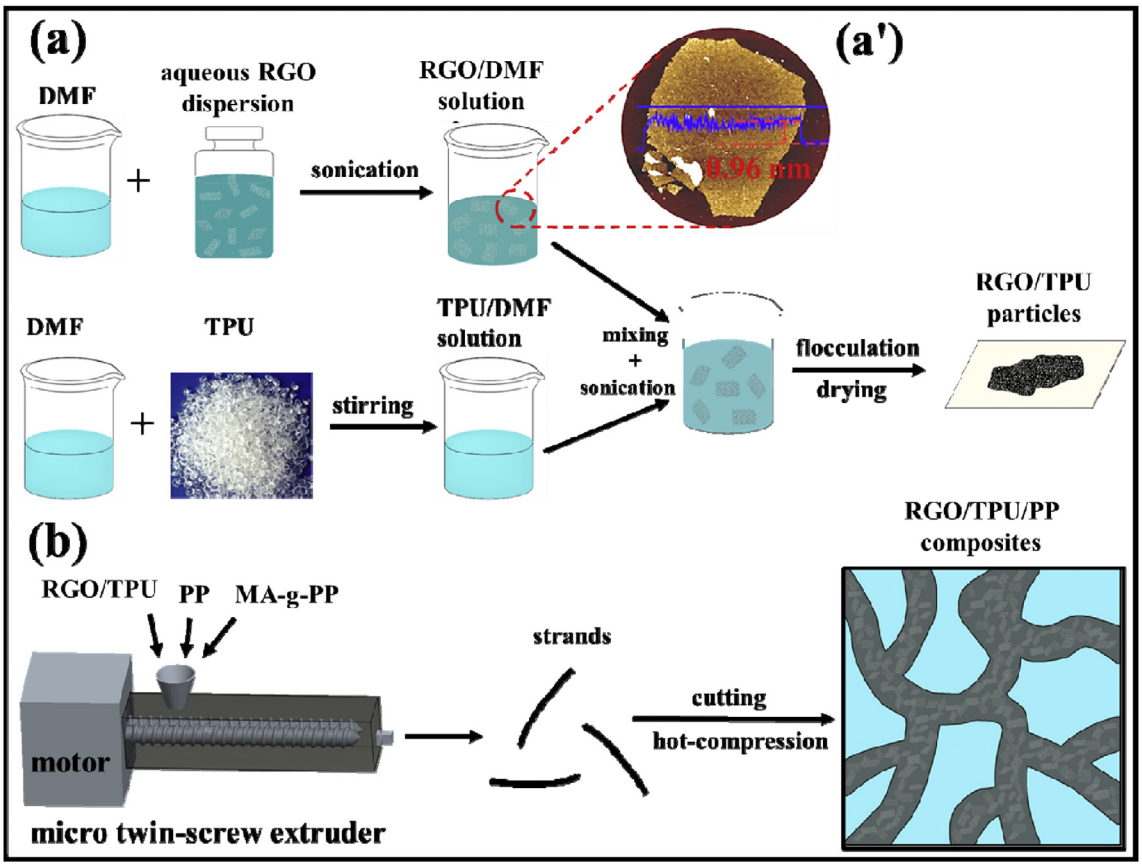

Fig. 1. Schematic illustration of the process for the preparation of RGO/TPU/PP composites by (a) solution-flocculation and (b) melt-mixing, (a′) is the non-tapping-mode AFM image of RGO.

with 0.5 wt% RGO, then it was impossible to prepare the RGO/TPU/PP composites by simple melt-mixing technique with aqueous RGO suspension, TPU and PP. Similarly, it was hardly possible for the PP particles to dissolve in DMF, hence simple solution-mixing with graphene, TPU and PP was not a desirable method to fabricate the RGO/TPU/PP composites. To sum up, the combination of solution-mixing and melt-mixing method, *i.e.* the solution-melt mixing technique, was the most suitable method to prepare RGO/TPU/PP composites.

2.3. Characterization

Atom force microscopy (AFM) images of RGO after sonication in DMF were taken in the non-tapping mode on a VEECO Nanoscope IV instrument. The specimens were prepared by spin-coating RGO solution on a mica plate and subsequently drying in a vacuum oven. The crystalline structures of TPU, PP, TPU/PP blend, and RGO/TPU/PP composites with various RGO contents were investigated by utilizing the wide-angle X-ray diffraction (WAXD) (Ultima IV, Rigaku Corporation). The surface energy of all components was calculated by the contact angle measurements, which were performed on the surface of compression-molded films of pure TPU and PP. The measurements of the contact angle of a given sample were carried out at least for five times. Distilled water (H_2O) and ethylene glycol ($C_2H_6O_2$) were used as probe liquids.

Optical microscope (OM) (BX51, OLYMPUS, Japan) and field emission scanning electron microscopy (FESEM) (JEOL JSM-7500F, Japan) were performed to characterize the microstructures of the RGO/TPU/PP composites. The specimen was cut into films with a thickness of about 10 μm by a microtome for optical microscope observation. The detailed information of the morphology was further investigated by FESEM with an accelerating voltage of 5 kV. For FESEM observation, the specimens were firstly cryogenically fractured in liquid nitrogen; and some samples were then etched by DMF for 2 h at ambient temperature to remove the TPU phase. All the specimens were sputter-coated with a thin layer of gold for better imaging. The transmission electron microscope (TEM) observations were performed on a JEOL JEM-1230 with an acceleration voltage of 90 kV. Before the observation, the samples were ultra-microtome into ultrathin films with a thickness of about ~100 nm in liquid nitrogen by a microtome (Leica UC-7) equipped with a glass knife.

The volume electrical resistivity lower than 10^6 Ω m was measured by four probe method, the volume resistivity higher than 10^6 Ω m was measured by a high-resistance meter. Copper meshes were attached to both sides of each sample to ensure good contacts between the samples and the electrodes. The dimension of the tested samples was 40 × 10 × 0.5 mm^3. The mechanical properties of RGO/TPU/PP composites were tested on Suns UTM2203 universal testing machine (with 100 N load cell) at a cross-head speed of 0.5 mm/min, and the gauge length was fixed at 16 mm. The tested samples with dimensions of 40 × 4 × 0.5 mm^3 were cut from the hot-compressed films for the mechanical performance test. Each type of samples had been carried out at least eight parallel measurements to make statistical analysis of the mechanical properties.

The viscosity of TPU and PP was measured on Malvern Rheometer (Bohlin Gemini 2, UK) with parallel-plate geometry (diameter of 25 mm). The testing samples were hot pressed into

disks with a thickness of 1 mm and diameter of 25 mm. Oscillatory frequency was swept from 0.1 to 100 rad/s with a fixed strain amplitude of 1% to ensure that the rheological behavior was located in the linear viscoelasticity regime, and the composites were tested at 200 °C under nitrogen atmosphere.

3. Results and discussion

To characterize the dispersion state of RGO in the polymer matrix, the wide-angle X-ray diffraction patterns of the hot-compressed films of TPU, PP, TPU/PP blend and the conductive composites with various RGO contents were investigated, Fig. 2. The TPU film exhibits only a broad diffraction peak ranging from 15 to 26° and centered at 21.2°, Fig. 2a, that can be assigned to polyether segment [19]. While the PP film exhibits sharp diffraction peaks associated with the α-form crystal, which is caused by the rapid crystallization during the melt-quenching process [20]. For the TPU/PP blend and its composite films with different RGO contents, X-ray diffraction patterns are almost identical to that of neat PP film. This indicates that the crystallization behavior is dominated by the α-form PP crystals developed during the melt-quenching process [21]. Importantly, the XRD patterns of the RGO/TPU/PP composites with various RGO contents, Fig. 2b, indicate that there are no distinct RGO characteristic peaks at 2θ ~24°. Accordingly, it can be inferred that RGO is well dispersed in the polymer matrix and there is no significant re-stacking of RGO nanosheets in the CPCs [22,23].

In order to investigate the morphological characteristics of the CPCs, the distribution of RGO in the TPU/PP blend is predicted firstly. Generally, selective dispersion of electrical conductive nanofillers in one specific phase or at the interface of immiscible polymer blend is mainly determined by the combined action of thermodynamic and kinetic factors [24]. The former relies on the wetting coefficient (ω_a), which can be theoretically deduced from Equation (1) [2]:

$$\omega_a = \frac{\gamma_{G-TPU} - \gamma_{G-PP}}{\gamma_{TPU-PP}} \tag{1}$$

where γ_{G-TPU}, γ_{G-PP} and γ_{TPU-PP} represent the interface energy between RGO and TPU, RGO and PP, and TPU and PP, respectively. If $\omega_a < -1$, RGO will preferentially locate in the TPU phase; if $\omega_a > 1$, RGO will preferentially locate in the PP phase; and if $-1 < \omega_a < 1$, RGO will locate at the interface between the matrix and the dispersed phase. The interface energy can be estimated by both Harmonic-mean equation (Eq. (2)) and Geometric-mean equation (Eq. (3)) [25]:

$$\gamma_{12} = \gamma_1 + \gamma_2 - 4\left(\frac{\gamma_1^d\gamma_2^d}{\gamma_1^d + \gamma_2^d} + \frac{\gamma_1^p\gamma_2^p}{\gamma_1^p\gamma_2^p}\right) \tag{2}$$

$$\gamma_{12} = \gamma_1 + \gamma_2 - 2\sqrt{\gamma_1^d\gamma_2^d} - 2\sqrt{\gamma_1^p\gamma_2^p} \tag{3}$$

where γ_1^d and γ_1^p represent the dispersive and polar parts of the surface tension of component 1, respectively. γ_1 is the surface energy of component 1, which can be calculated by the contact angle according to Eq. (4):

$$\gamma_l(1 + \cos\theta) = 2\sqrt{\gamma_s^d \cdot \gamma_l^d} + 2\sqrt{\gamma_s^p \cdot \gamma_l^p} \tag{4}$$

where θ is the contact angle; γ_s and γ_l denote the surface energies of solid and liquid. The contact angles of the TPU films for distilled H_2O and $C_2H_6O_2$ are 78.5° and 58.6°, the PP films for distilled H_2O and $C_2H_6O_2$ are 83.6° and 54.8°, respectively. Table 1 shows the corresponding surface energy data of TPU and PP.

For the RGO, the surface energy is calculated by the Owens-Wendt model [26]:

$$\frac{\gamma_l(1 + \cos\theta)}{2\sqrt{\gamma_l^d}} = \sqrt{\gamma_s^p}\,\frac{\gamma_l^p}{\gamma_l^d} + \gamma_s^d \tag{5}$$

where γ_l^d and γ_l^p are the dispersive and polar parts of the liquid, γ_s^d and γ_s^p are the dispersive and polar parts of the solid, respectively. The average contact angles of graphene films for water and ethylene glycol are reported to be about 127.0° and 76.3° respectively [27]. The surface energy of RGO is calculated to be 15.3 mJ/m^2, and the dispersive and polar parts of the surface energy are 4.1 and 11.2 mJ/m^2, respectively.

Based on the data of surface energy of TPU, PP and RGO, using Eq. (2) and Eq. (3), the corresponding interfacial energy is calculated and listed in Table 2. According to the data of interfacial energy and Eq. (1), ω_a are −2.0 or −2.3 based on Harmonic-mean equation or Geometric-mean equation. Therefore, the theoretically thermodynamic calculation indicates that RGO tends to be preferentially located in the TPU phase during the melt-mixing process.

Table 1
Surface energy data of the components.

Component	γ^p (mJ/m^2)	γ^d (mJ/m^2)	γ (mJ/m^2)	References
TPU	12.6	15.4	28.0	
PP	5.1	27.2	32.3	
RGO	11.2	4.1	15.3	[24,25]

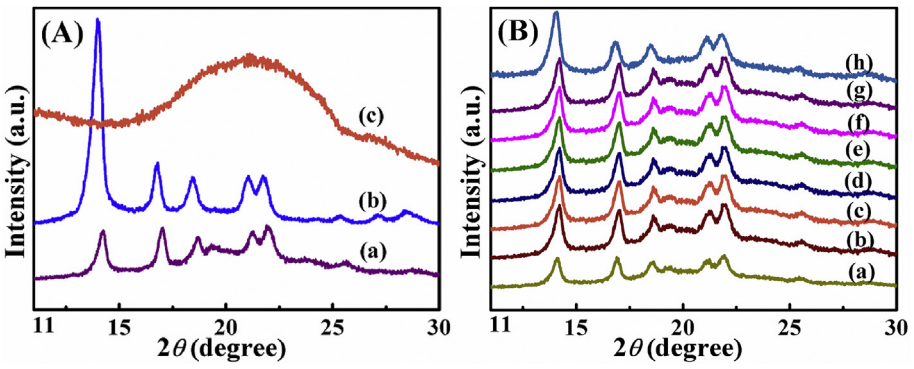

Fig. 2. X-ray diffraction patterns of (A) (a) TPU, (b) PP and (c) TPU/PP; and (B) RGO/TPU/PP composites with a RGO loading of (a) 0.05, (b) 0.1, (c) 0.3, (d) 0.5, (e) 0.7, (f) 1.0, (g) 1.2 and (h) 1.5 wt%.

Table 2
Interfacial energy as calculated by Harmonic-mean equation and Geometric-mean equation.

Samples	Based on Harmonic-mean equation (mJ/m^2)	Based on Geometric-mean equation (mJ/m^2)
RGO/TPU	6.7	3.7
RGO/PP	19.4	11.4
TPU/PP	6.3	3.3

The melt viscosity is another key factor influencing the distribution of conductive fillers in an immiscible blend [24,28–30]. Fig. 3 shows the melt viscosity of pure TPU and PP as a function of angle frequency. It is obvious that the melt viscosity of TPU is much lower than that of PP within the experiment range. The shear rate applied in the melt-mixing process was 50 rpm, which was estimated to be 5.24 rad/s according to the conversion law: 1 rad/s = 9.55 rpm. Based on the literature, the nanofillers are reported to have a tendency to localize in the lower viscosity phase [2,24]. Therefore, from the kinetics point of view, it is suggested that RGO is preferentially distributed in the TPU phase during the melt-mixing process. Additionally, the processing design plays an important role in determining the selective location of the nanofillers. In terms of the preparation techniques (RGO was premixed with TPU) and the intrinsic characteristics of RGO, it is unlikely for RGO to transfer from TPU phase to PP phase during the melt-mixing procedure due to its high specific surface area and large size.

On the whole, thermodynamic factor, the kinetic factor and the sample preparation procedure are all important for the selective distribution of RGO in the composites. Nevertheless, it is believed that the thermodynamic factor is the determining factor. According to Table 2, it is evident that the interfacial energy between the RGO and TPU is much lower than that of the RGO and PP. This indicates that the TPU shows much stronger thermodynamic affinity to RGO than PP. Therefore, from the viewpoint of thermodynamics, the RGO tends to locate in the TPU phase. Meanwhile, the melt viscosity of PP is apparent higher than that of TPU. In addition, RGO was premixed with TPU and then melt mixed with PP. Therefore, all the factors were beneficial for the selective dispersion of RGO in the TPU phase. Considering the large size of RGO, it is almost impossible for RGO to migrate from the low viscosity TPU phase to the high viscosity PP phase during the melt mixing process. In a word, the RGO tend to distribute in the TPU phase preferentially through the combined action of thermodynamic and kinetic factors. Among them, the thermodynamic factor is the determining factor.

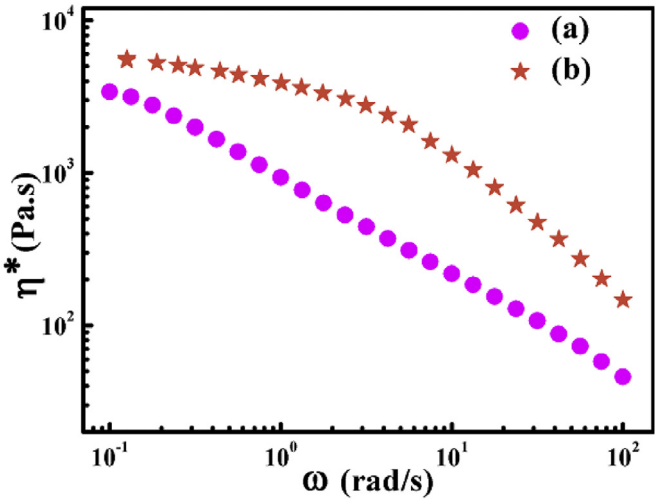

Fig. 3. Complex viscosity of (a) TPU and (b) PP.

Fig. 4 shows the optical images of the RGO/TPU/PP composites, which provide insight into the microstructure of the composites. A typical co-continuous structure can be observed, Fig. 4. It is deduced that the light and dark domains correspond to the PP and RGO/TPU phase, respectively, based on the aforementioned analysis. It is obvious that most of the RGO have been selectively resided in the TPU phase while no RGO are observed in the PP phase.

Fig. 5 shows the TEM microstructures of the RGO/TPU/PP composites with RGO content of 1.0 wt%. A typical two-phase structure is formed in the composites, Fig. 5(a) and (b). The RGO nanosheets are selectively located in the TPU phase, and no obvious RGO nanosheets are found in the PP phase. The results agree well with the theoretical predictions and the OM, SEM observations. The selective location of RGO in TPU is mainly determined by the combined action of thermodynamic and kinetic factors. In addition, the RGO nanosheets are dispersed homogeneously in the TPU phase without obvious aggregation, Fig. 5(c) and (d).

The dispersion state of RGO nanosheets in the matrix can be studied further from the fractured surfaces. Fig. 6 illustrates the fracture surfaces of the RGO/TPU/PP composites. No obvious phase interface between TPU and PP phase can be differentiated, Fig. 6a. It is mainly ascribed to the addition of compatibilizer, which efficiently enhances the interfacial adhesion of the two matrices. RGO nanosheets with wrinkled structure and large-size can be discerned, Fig. 6b. Obviously, the RGO nanosheets are combined well with the TPU matrix.

To provide clearer insights into the co-continuous structure and the RGO distribution in the composites, FESEM micrographs of the RGO/TPU/PP composites after etching by DMF are shown in Fig. 7. Apparently, the composites show a nice co-continuous structure, which is coincident with the above optical microscope results quite well. Due to the nice solubility of TPU in DMF, it is understandable that the TPU phase has been dissolved after this processing. Furthermore, the surface of PP phase is very smooth and no wrinkle structure of RGO nanosheets can be differentiated, Fig. 7b, indicating that RGO have also been removed from the CPC. This reveals

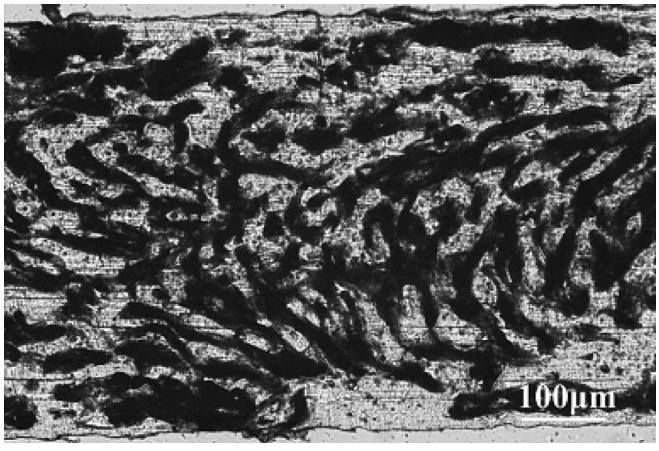

Fig. 4. Optical images of RGO/TPU/PP composite, the content of RGO is 1.0 wt% for the observation of typical co-continuous structure and conductive network.

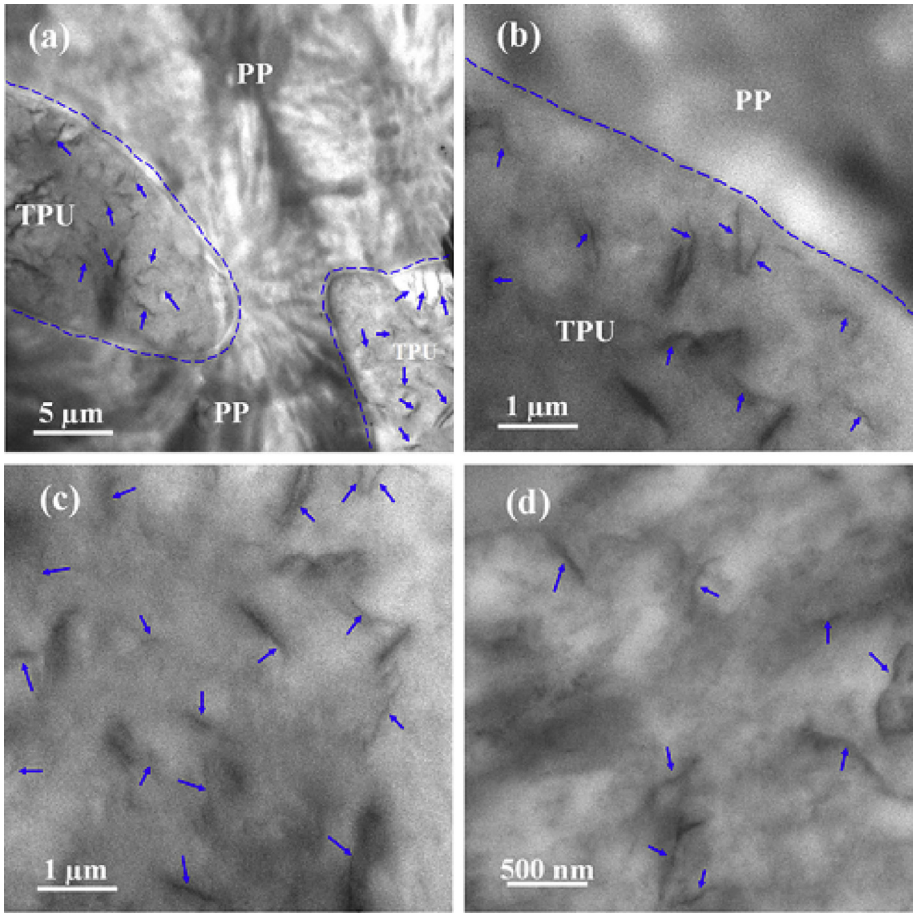

Fig. 5. TEM images of 1.0 wt% RGO/TPU/PP composite.

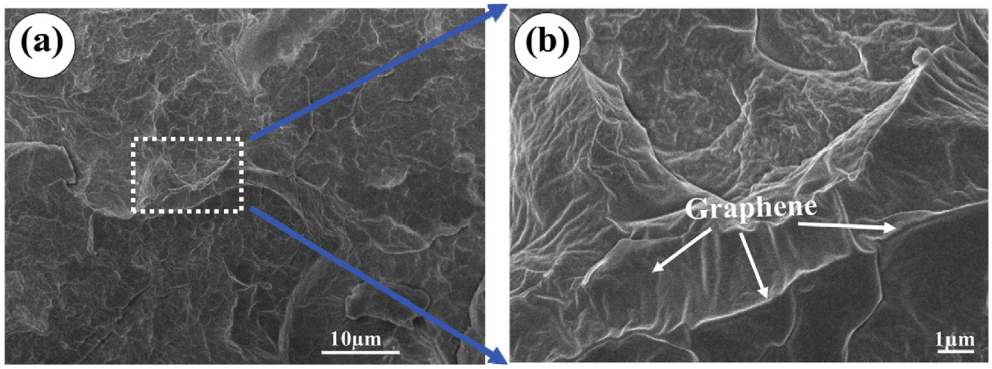

Fig. 6. SEM images of fractured surface of 1.2 wt% RGO/TPU/PP composite.

again that the RGO are preferentially accumulated in the TPU phase [31]. Hence, we can conclude that most of the RGO have been located in the TPU phase and there is no obvious migration of RGO occurring from TPU to PP phase in the course of sample preparation.

Fig. 8 shows the electrical conductivity of the composites as a function of the RGO content. The conductivity shows a sharp rise of about 6 orders of magnitude as the RGO content increases from 0 to 0.5 wt%, indicating that a good percolation conductive network is formed in the composites. The electrical conductivity of the composites above the percolation threshold is predicated by the statistical percolation model as shown in Eq. (6) [32].

$$\sigma \propto (\phi\text{-}\phi_c)^t \quad \text{for } \phi > \phi_c, \tag{6}$$

where σ is the electrical conductivity of the composites, ϕ is the weight fraction of RGO, ϕ_c is the percolation threshold, t is the critical exponent that depends on the dimensionality of the percolation network. The percolation threshold is estimated from the curves to be 0.054 wt%, which is much lower than that of graphene/TPU ($\phi_c = 0.1$ wt%) [33] and graphene/PP ($\phi_c = 0.4$ wt%) [34]. It is believed that the very low percolation threshold is the result of the joint action of the co-continuous structure and the selective location of highly conductive RGO with a high SSA.

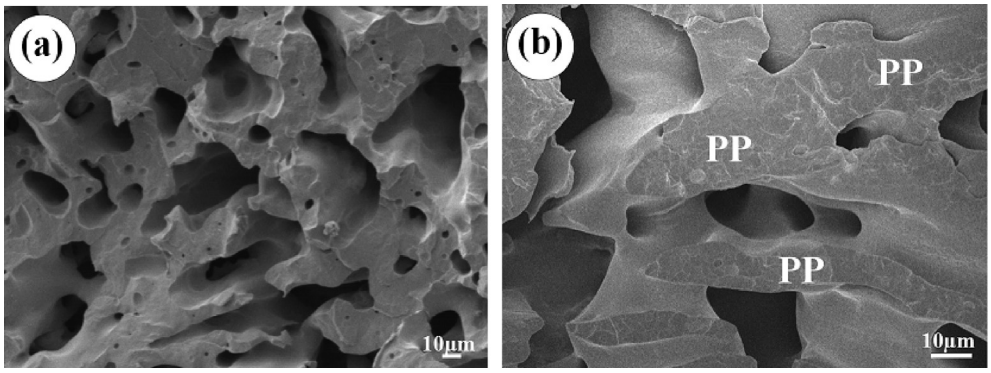

Fig. 7. (a) SEM images of the morphology of 1.0 wt% RGO/TPU/PP composite, (b) SEM images of 1.0 wt% RGO/TPU/PP composite at high magnification. TPU phase was removed by using DMF.

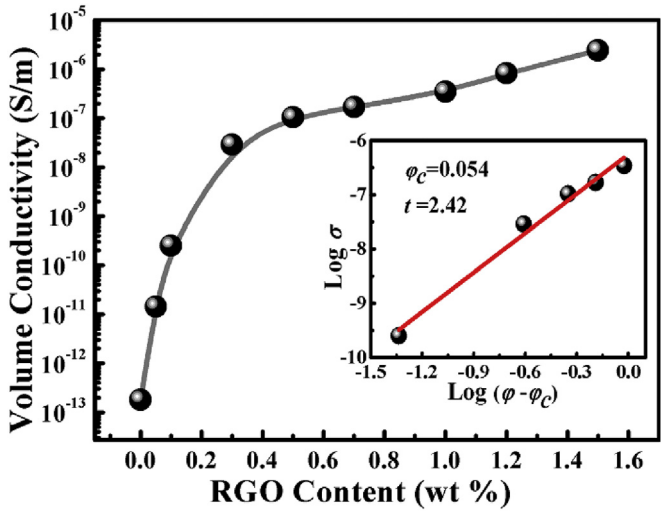

Fig. 8. Electrical conductivity as a function of RGO content for RGO/TPU/PP composites, the inset shows a log-log plot of the conductivity as a function of $(\phi - \phi_c)$ with an exponent $t = 2.42$ and a critical weight content $\phi_c = 0.054$ wt %.

The insert of Fig. 8 shows the double-logarithmic plot of the electrical conductivity versus $(\phi - \phi_c)$. Using the data in Fig. 8, t is estimated to be 2.42. It is well known that the value of t varied in the range of 1.6–2.0 means a three-dimensional network [35,36]. The obtained higher value of t (2.42) here implies a complicated conductive network in the composites. It is possible that the higher value of t relates to the high SSA of RGO nanosheets, the selective location of RGO and the complex morphology of the composites [29]. The high value of t has also been reported in others literature [37–39].

The nanofiller's concentration, dispersion state and the interaction between matrix and the nanofiller influence the composites' mechanical properties crucially. Fig. 9 presents the bar diagrams of tensile strength (it refers to the stress at break) and elongation at break *vs.* RGO concentration, respectively. The results of uniaxial tensile test show a non-monotonic trend of the mechanical property with the filler loading. In case of RGO concentration increasing from 0 to 0.5 wt%, both the tensile strength and the elongation at break increase simultaneously. When the RGO concentration further increases to 1.2 wt%, the tensile strength and the elongation at break decrease simultaneously instead. In other words, when RGO concentration in the composites approaches 0.5 wt%, the tensile strength and the elongation of the RGO/TPU/PP composites achieved an optimal value of 11.89 MPa and 16.08%, which is improved by 341.9% and 354.3% as compared to that of the TPU/PP composites.

It is interesting to note that the mechanical analysis of the RGO/TPU/PP composites appears to differ from the conventional composites system, in which the tensile strength increases with increasing the filler concentration while the elongation at break decreases [40]. It is believed that the enhancement of tensile strength without sacrificing the toughness is mainly stemmed from excellent mechanical strength of RGO, good dispersion of RGO in the matrix, and strong interfacial interactions between the two components with the help of compatibilizer. Nice interfacial adhesion between RGO and TPU is also important. During the tensile test, the effective stress transfer from the matrix polymer to RGO is beneficial to the reinforcement of the composites [41,42].

When the RGO concentration is over 0.5 wt%, the tensile strength gets deteriorated, Fig. 9a. It is supposed that the RGO nanosheets are vulnerable to aggregation at high RGO contents. Moreover, the van der Waals interaction between the RGO nanosheets will relatively weaken the interaction between the matrix and RGO available for the stress transfer [43,44]. Meanwhile, the elongation at break of the composites decreases as well, Fig. 9b, and it is attributed to the limited deformation degree of molecular chains of TPU at higher RGO content [45]. In addition, it is possible that the variation of RGO concentration might cause the transition of morphology to some extent, affecting the mechanical performances evolution in turn [46]. The morphology changes of the composites are illustrated in Fig. 10, showing the optical images of the composites with various RGO concentrations. It is easy to differentiate the two phases from the optical images, namely, all the composites exhibit a similar co-continuous structure with the RGO selectively located in the TPU phase. In other words, the variation of RGO concentration does not change the co-continuous structure of the composites. However, it is worth mentioning that the co-continuous structure becomes more obvious and finer with increasing the RGO content. For another, the RGO results in the change of phase domains of PP and TPU, *i.e.* the phase domains of PP and TPU decrease with increasing the RGO concentration. Similar morphology changes have been reported previously [47–49] and are mainly related to the RGO content and the viscosity ratio between the polymer components. Jordhamo and co-workers [50] predict the point of phase inversion following Eq. (7).

$$\frac{\eta_1}{\eta_2}\cdot\frac{\varphi_2}{\varphi_1} = 1 \tag{7}$$

where, η_1 and η_2 represent the viscosity of two polymer components, respectively, ϕ_1 and ϕ_2 are the content of the polymer

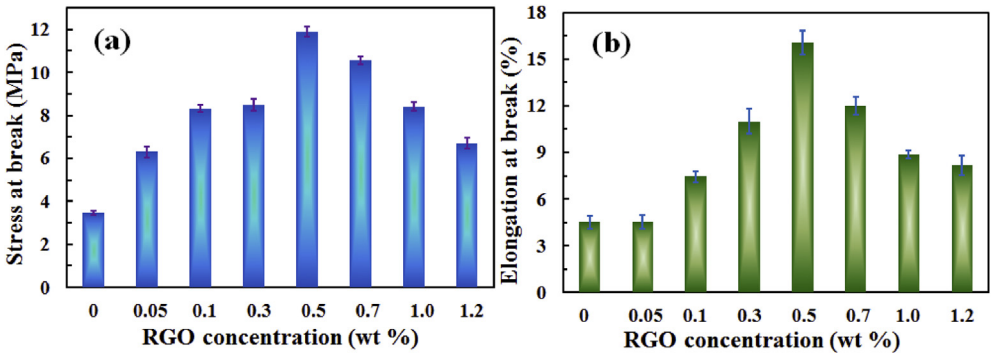

Fig. 9. Bar diagrams of (a) tensile strength and (b) elongation at break of RGO/TPU/PP composites with various graphene loadings.

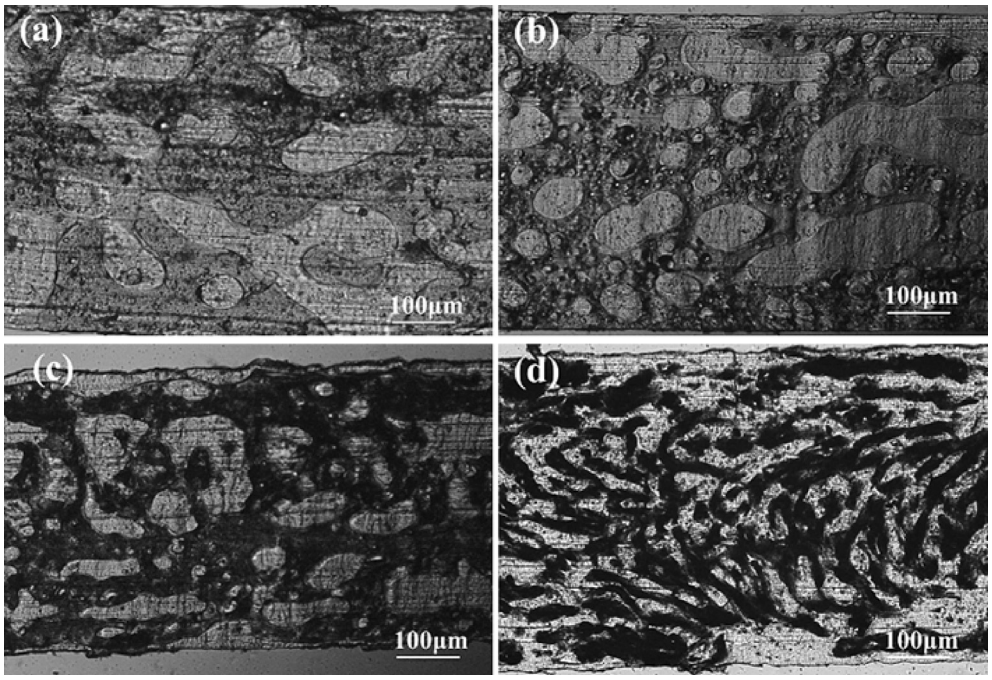

Fig. 10. Optical images of RGO/TPU/PP composites with various RGO contents, (a) 0.05, (b) 0.1, (c) 0.5, and (d) 1.0 wt% RGO/TPU/PP composites.

components, respectively. When the compositions of the components are invariable, the blend morphology is mainly determined by the viscosity ratio. Zou et al. [51] describe the change of blend morphology with different contents of CNTs in poly(*p*-phenylenesulfide)/polyamide66 (PPS/PA66, 60w/40w) system. The PPS/PA66 blend shows typical sea-island morphology. However, the phase morphology changes from sea-island to co-continuous structure when adding small amount of CNTs (0.01–0.3 phr). The co-continuous morphology returns back to sea-island structure when the CNTs content further increases to 0.5 and 1 phr.

In this work, MA-g-PP induces the slight decrease of the viscosity of PP component. Undoubtedly, the viscosity of the filled TPU improves with the increase of RGO content, leading to the obviously increased viscosity of the composites, Fig. S1. Thus, the viscosity ratio between filled TPU and PP also increases with the increase of the RGO content. The increased TPU viscosity induces higher shear stress, which then breaks up the PP component and results in a reduced size of the PP. At the same time, the coalescence of filled TPU becomes impeded, resulting in smaller structures of the RGO filled TPU component within the unfilled PP phase [15]. Therefore, the domain sizes of TPU and PP phase decrease, and the amount of conductive RGO/TPU branch increases. Certainly, the coalescence of the broken domains also takes place to some extent. Finally, a more obvious and finer co-continuous structure is formed in the composites with the increase of RGO content.

For the conductive properties, with the increase of RGO content, the decreased domain sizes of the TPU and PP phases in the nanocomposites are observed gradually. More conductive paths are constructed in the TPU phase with a developed microstructure in the nanocomposites, therefore, the conductivity is greatly improved and a sharp rise more than 6 orders of magnitude as the RGO content increases from 0 to 1 wt% is displayed. The morphology evolution also influences the mechanical properties of the composites to some extent. The total contact area between TPU and PP increases with the decrease of domain size of TPU and PP phases, the interaction between TPU and PP would thus be improved. The effective stress transfer between TPU and RGO also contributes to the reinforcement of the composites. The mechanical properties of the nanocomposites are enhanced significantly when the RGO content increases from 0 to 0.5 wt%. When the RGO content is over 0.5 wt%, the aggregation of RGO weakens the effect of stress transfer and limits the deformation degree of molecular

chains of TPU, resulting in the deterioration of the mechanical properties.

4. Conclusions

RGO with high electrical conductivity was introduced to the immiscible TPU/PP blend by solution-flocculation and melt-mixing process. X-ray diffraction patterns manifested that RGO was well-dispersed in the matrix and α-form crystals of PP were developed dominantly in the polymer composites. The optical microscope and FESEM images affirmed the fact that a nice co-continuous structure in the immiscible polymer composites was formed and RGO was selectively resided in the TPU phase. TEM measurements provided more direct observations of selective location and homogeneous dispersion of RGO in the TPU phase. Based on the formation of co-continuous structure and the selective location of RGO, a conductive composite with a very low percolation concentration of 0.054 wt% was achieved. Mechanical property tests showed that the tensile strength and the elongation at break emerged a maximum value at the RGO contents of 0.5 wt%. The morphology evolution had been further investigated to illustrate the changes of mechanical, electrical properties. The morphology evolution of the composites was mainly ascribed to the change of viscosity ratio and RGO content. The preparation method, *i.e.* solution-flocculation and melt-mixing process through a micron twin-screw extruder, combines the advantage of nice dispersion of RGO, good conductive and mechanical properties and improved processing efficiency of the composites. This technique can also be applied to fabricate other similar graphene based immiscible polymer composite systems. This paper reveals that the employment of efficiently industrial techniques (*i.e.*, extrusion) for preparing graphene based CPCs could bridge the gap from nanoscience and nanoengineering to a large-scale production of graphene based polymer composites with reliable and tunable properties for practical applications.

Acknowledgements

The authors gratefully acknowledge the financial support of this work by National Natural Science Foundation Item (Contract Number: 11572290, 11432003), China Postdoctoral Science Foundation (Contract Number: 2015M580637), Special Science Foundation for Excellent Youth Scholars of Zhengzhou University (Contract Number 1421320041) and National Program on Key Basic Research Project (973 Program, Contract Number: 2012CB025903). Z. Guo appreciates the start - up funds from University of Tennessee.

Appendix A. Supplementary data

Supplementary data related to this article can be found at http://dx.doi.org/10.1016/j.polymer.2016.05.017

References

[1] H. Kim, A.A. Abdala, C.W. Macosko, Macromolecules 43 (16) (2010) 6515–6530.
[2] M. Sumita, K. Sakata, S. Asai, K. Miyasaka, H. Nakagawa, Polym. Bull. 25 (2) (1991) 265–271.
[3] F. Gubbels, R. Jérôme, P. Teyssie, E. Vanlathem, R. Deltour, A. Calderone, V. Parente, J.-L. Brédas, Macromolecules 27 (7) (1994) 1972–1974.
[4] F. Gubbels, R. Jérôme, E. Vanlathem, R. Deltour, S. Blacher, F. Brouers, Chem. Mater. 10 (5) (1998) 1227–1235.
[5] E. Segal, R. Tchoudakov, M. Narkis, A. Siegmann, J. Polym. Sci. Part B Polym. Phys. 41 (12) (2003) 1428–1440.
[6] W. Thongruang, C.M. Balik, R.J. Spontak, J. Polym. Sci. Part B Polym. Phys. 40 (10) (2002) 1013–1025.
[7] J. Chen, Y.-y. Shi, J.-h. Yang, N. Zhang, T. Huang, C. Chen, Y. Wang, Z.-w. Zhou, J. Mater. Chem. 22 (42) (2012) 22398–22404.
[8] X. Gao, S. Zhang, F. Mai, L. Lin, Y. Deng, H. Deng, Q. Fu, J. Mater. Chem. 21 (17) (2011) 6401–6408.
[9] J. Huang, C. Mao, Y. Zhu, W. Jiang, X. Yang, Carbon 73 (2014) 267–274.
[10] Y. Li, H. Shimizu, Macromolecules 41 (14) (2008) 5339–5344.
[11] D. Mi, K. Liu, H. Du, J. Zhang, Polym. Adv. Technol. 25 (4) (2014) 364–371.
[12] P. Pötschke, A.R. Bhattacharyya, A. Janke, Polymer 44 (26) (2003) 8061–8069.
[13] M. Gültner, A. Göldel, P. Pötschke, Compos. Sci. Technol. 72 (1) (2011) 41–48.
[14] J. Plattier, L. Benyahia, M. Dorget, F. Niepceron, J.-F. Tassin, Polymer 59 (2015) 260–269.
[15] M. Liebscher, M.-O. Blais, P. Pötschke, G. Heinrich, Polymer 54 (21) (2013) 5875–5882.
[16] C. Mao, Y. Zhu, W. Jiang, ACS Appl. Mater. Interfaces 4 (10) (2012) 5281–5286.
[17] X.-Y. Qi, D. Yan, Z. Jiang, Y.-K. Cao, Z.-Z. Yu, F. Yavari, N. Koratkar, ACS Appl. Mater. Interfaces 3 (8) (2011) 3130–3133.
[18] R. Rohini, S. Bose, ACS Appl. Mater. Interfaces 6 (14) (2014) 11302–11310.
[19] A.V. Raghu, Y.R. Lee, H.M. Jeong, C.M. Shin, Macromol. Chem. Phys. 209 (24) (2008) 2487–2493.
[20] S. Liu, Y. Liang, Y. Quan, K. Dai, G. Zheng, C. Liu, J. Chen, C. Shen, Polymer 54 (12) (2013) 3117–3123.
[21] T.-W. Lee, Y.G. Jeong, Compos. Sci. Technol. 103 (2014) 78–84.
[22] X. Li, H. Deng, Z. Li, H. Xiu, X. Qi, Q. Zhang, K. Wang, F. Chen, Q. Fu, Compos. Part A Appl. Sci. Manuf. 68 (2015) 264–275.
[23] K.-H. Liao, Y.T. Park, A. Abdala, C. Macosko, Polymer 54 (17) (2013) 4555–4559.
[24] Y.-y. Shi, J.-h. Yang, T. Huang, N. Zhang, C. Chen, Y. Wang, Compos. Part B Eng. 55 (2013) 463–469.
[25] S. Wu, Polymer Interface and Adhesion, M. Dekker, 1982.
[26] D.K. Owens, R. Wendt, J. Appl. Polym. Sci. 13 (8) (1969) 1741–1747.
[27] S. Wang, Y. Zhang, N. Abidi, L. Cabrales, Langmuir 25 (18) (2009) 11078–11081.
[28] J. Feng, C.M. Chan, J.X. Li, Polym. Eng. Sci. 43 (5) (2003) 1058–1063.
[29] F. Gubbels, S. Blacher, E. Vanlathem, R. Jérôme, R. Deltour, F. Brouers, P. Teyssie, Macromolecules 28 (5) (1995) 1559–1566.
[30] P. Zhou, W. Yu, C. Zhou, F. Liu, L. Hou, J. Wang, J. Appl. Polym. Sci. 103 (1) (2007) 487–492.
[31] C. Zhang, X.-S. Yi, H. Yui, S. Asai, M. Sumita, Mater. Lett. 36 (1) (1998) 186–190.
[32] A. Aharony, D. Stauffer, Introduction to Percolation Theory, Taylor & Francis, 2003.
[33] H. Liu, Y. Li, K. Dai, G. Zheng, C. Liu, C. Shen, X. Yan, J. Guo, Z. Guo, J. Mater. Chem. C 4 (1) (2016) 157–166.
[34] Y.V. Syurik, M.G. Ghislandi, E.E. Tkalya, G. Paterson, D. McGrouther, O.A. Ageev, J. Loos, Macromol. Chem. Phys. 213 (12) (2012) 1251–1258.
[35] R. Fisch, A.B. Harris, Phys. Rev. B 18 (1) (1978) 416.
[36] J.P. Straley, Phys. Rev. B 15 (12) (1977) 5733.
[37] C. Gao, S. Zhang, F. Wang, B. Wen, C. Han, Y. Ding, M. Yang, ACS Appl. Mater. Interfaces 6 (15) (2014) 12252–12260.
[38] S. Stankovich, D.A. Dikin, G.H. Dommett, K.M. Kohlhaas, E.J. Zimney, E.A. Stach, R.D. Piner, S.T. Nguyen, R.S. Ruoff, Nature 442 (7100) (2006) 282–286.
[39] H.-B. Zhang, W.-G. Zheng, Q. Yan, Y. Yang, J.-W. Wang, Z.-H. Lu, G.-Y. Ji, Z.-Z. Yu, Polymer 51 (5) (2010) 1191–1196.
[40] C. Bora, P. Bharali, S. Baglari, S.K. Dolui, B.K. Konwar, Compos. Sci. Technol. 87 (2013) 1–7.
[41] R.K. Layek, A.K. Das, M.J. Park, N.H. Kim, J.H. Lee, Carbon 81 (2015) 329–338.
[42] X. Zhao, Q. Zhang, D. Chen, P. Lu, Macromolecules 43 (5) (2010) 2357–2363.
[43] I.M. Inuwa, A. Hassan, S.A. Samsudin, M. Kassim, M. Haafiz, M. Jawaid, Polym. Compos. 35 (10) (2014) 2029–2035.
[44] Y. Liu, H. Wu, G. Chen, Polym. Compos. 37 (4) (2016) 1190–1197.
[45] M. Liu, C. Zhang, W.W. Tjiu, Z. Yang, W. Wang, T. Liu, Polymer 54 (12) (2013) 3124–3130.
[46] Wang Yh, Shi Yy, J. Dai, Yang Jh, T. Huang, N. Zhang, Y. Peng, Y. Wang, Polym. Int. 62 (6) (2013) 957–965.
[47] J. Chen, H.-y. Lu, J.-h. Yang, Y. Wang, X.-t. Zheng, C.-l. Zhang, G.-p. Yuan, Compos. Sci. Technol. 94 (2014) 30–38.
[48] Y. Li, H. Shimizu, Macromol. Rapid Commun. 26 (9) (2005) 710–715.
[49] Y. Li, H. Shimizu, Polymer 45 (22) (2004) 7381–7388.
[50] G.M. Jordhamo, J.A. Manson, L.H. Sperling, Polym. Eng. Sci. 26 (8) (1986) 517.
[51] H. Zou, K. Wang, Q. Zhang, Q. Fu, Polymer 47 (22) (2006) 7821–7826.